Weather and Climate Extremes 40 (2023) 100566

Contents lists available at ScienceDirect

Weather and Climate Extremes

journal homepage: www.elsevier.com/locate/wace

Quantifying hazard of drought and heat compound extreme events during maize (Zea mays L.) growing season using Magnitude Index and Copula

Ying Guo [a,b,c], Jiquan Zhang [a,b,c,*], Kaiwei Li [a,b,c], Han Aru [a,b,c], Zhi Feng [a,b,c], Xingpeng Liu [a,b,c], Zhijun Tong [a,b,c]

[a] School of Environment, Northeast Normal University, Changchun, 130024, China
[b] State Environmental Protection Key Laboratory of Wetland Ecology and Vegetation Restoration, Northeast Normal University, Changchun, 130024, China
[c] Key Laboratory for Vegetation Ecology, Ministry of Education, Changchun, 130024, China

ARTICLE INFO

Keywords:
Compound event
Hazard assessment
Drought
Heat
Copula
Conditional cumulative probability

ABSTRACT

Hazard assessment is the basic work in the field of disaster risk. For the agricultural field which is seriously affected by extreme events, it is necessary to carry out hazard assessment of compound extreme events (CEEs) to increase the accuracy of risk assessment. First, in this study, the SMDI and TCI were used to characterize the spatial and temporal distribution patterns of agricultural drought and heat, respectively, and the drought and heat compound extreme events (DHCEEs) were identified by characterizing the drought and heat events based on runs theory. Then, the compound event magnitude index (CEMI) was constructed by fitting the non-transcendent probabilities. next, the optimal copula function of severity and duration of DHCEEs was screened, and the fitted probabilities were used in the hazard assessment. The hazard assessment model of DHCEEs is constructed by considering the occurrence probability, severity, and duration. We evaluated the hazard of all DHCEEs identified in the Songliao Plain from 1990 to 2020. The results show that the whole study area is affected by agricultural drought, and heat mainly affects the western region. CEMI can effectively determine the severity of DHCEEs. In the study area, 46.51% of the DHCEEs have a hazard less than 0.1, and 2.71% have a hazard greater than 0.5. The event that had the biggest hazard occurred in 2001, and the proportion of high hazard compound events gradually increased after 2000. Similar compound extreme events are gaining attention in important food-producing regions around the world, and the hazard assessment model constructed in this study can be used to assess crop damage from compound extreme events in real-time, increasing the relevance and accuracy of risk assessment.

1. Introduction

As one of the most typical extreme compound events, drought and heat compound extreme events (DHCEEs) bring escalating threats to agricultural production (Hammer et al., 2020; Lobell et al., 2015; Mehrabi and Ramankutty, 2017), but the extent to which current risk assessments of compound extreme events (CEEs) can reflect such impacts is unclear (Curt, 2021; Kappes et al., 2012). With regional and global warming, drought and heat events are becoming more frequent, causing significant impacts on crops including, but not limited to, planted and harvested acreage, yields, planting boundaries, and resulting economic losses (Haqiqi et al., 2021; Sánchez et al., 2014; Teixeira et al., 2013; Waqas et al., 2021). Therefore, risk assessment of crops affected by DHCEEs is widely concerned (Hao and Singh, 2020). For vulnerable long-term rain-fed agricultural mechanisms, targeted hazard assessment of CEEs is more accurate to understand the impact of climate change on crops, which is important for early warning and prevention and control of extreme events (Merz et al., 2020; Ward et al., 2020).

Drought, a common agro-meteorological disaster, is a key climatic extreme that causes food production losses and thus spikes in food prices

Abbreviations: **DHCEEs**, drought and heat compound extreme events; **CEEs**, compound extreme events; **SMDI**, Soil Moisture Deficit Index; **TCI**, Temperature Condition Index; **CEMI**, Compound event magnitude index; **H**, Hazard of compound extreme events; **ts**, start time; **te**, end time; **GOF**, goodness of fit; **AIC**, Akaike Information Criterion; **RMSE**, Root Mean Squared Error.

* Corresponding author. Northeast Normal University, 2555 Jingyue Street, Changchun City, Jilin Province, China.
E-mail addresses: guoy471@nenu.edu.cn (Y. Guo), zhangjq022@nenu.edu.cn (J. Zhang), likw395@nenu.edu.cn (K. Li), arh690@nenu.edu.cn (H. Aru), fengz853@nenu.edu.cn (Z. Feng), liuxp912@nenu.edu.cn (X. Liu), gis@nenu.edu.cn (Z. Tong).

https://doi.org/10.1016/j.wace.2023.100566
Received 18 July 2022; Received in revised form 18 April 2023; Accepted 27 April 2023
Available online 27 April 2023

(Leng and Hall, 2019). between 1964 and 2007, global drought events caused losses of 1.82 billion mg, approximately equal to global maize and wheat production in 2013 (Leng and Hall, 2019). In agriculture, many studies related to drought or heat have been conducted based on deterministic and probabilistic methods. For example, Sheffield et al. (2009) conducted a severity-area-duration (SAD) analysis of drought events to identify and characterize the most severe events across continents and at different durations and spatial scales globally. Liu et al. (2019) analyzed the mechanism of constructing the composite drought index by the principal component analysis (PCA) and joint probability distribution methods, respectively. Mirabbasi et al. (2012) analyzed the frequency of drought events in northwestern Iran during 1967–2007 based on the standardized precipitation index combined with the Gumbel-copula function. Teixeira et al. (2013) conducted the first spatial assessment of global heat stress risk for four major crops, wheat, maize, rice, and soybean, based on heat stress intensity indices.

Drought and heat events cannot be studied without the construction of indicators, and various indices have been developed according to different fields such as meteorology, agriculture, and hydrology (Zargar et al., 2011). The heat indexes are centered on temperature thresholds, harmful accumulation temperatures, and temperature cycles (El Sabagh et al., 2019; Eyshi Rezaei et al., 2015). It is worth noting that heat and drought are two related but distinct factors, and regional land-air interactions sometimes significantly influence the development of CEEs, resulting in mutually reinforcing positive feedback effects. In the United States, extreme heat and drought have become two major limiting factors for rainfed corn cultivation systems (Li et al., 2022). In 2018, crop losses reached €340 million in Germany and €116 million in Switzerland when the continent experienced record-breaking summer heat and extreme drought (Bastos et al., 2020). Shi et al. (2021) used the SPI index and daily maximum temperature to investigate the spatial and temporal variability of drought and heat compound events in China, and found a general increase in heat wave-drought compound events in northern, northwestern, and southwestern China. Wang et al. (2018) used SPEI and extreme degree days to investigate the spatial and temporal distribution of drought and extreme heat in the Yellow-Huaihai Plain of China from 1981 to 2015, as well as the trends of compound extreme events. It is of concern that previous studies have often recognized and evaluated drought and heat events in isolation, without considering their interactions. And the studies mostly stop at spatial and temporal distribution pattern analysis or occurrence probability analysis.

Risk is the result of the interaction of hazard, exposure, and vulnerability. Hazard evaluation is the first step of disaster risk evaluation, which mainly measures the intensity of the causative factor to the hazard-bearing body. As a natural attribute of risk formation, hazard is the product of the probability of occurrence of an event and its severity (Chunyi et al., 2015). As an essential work for agro-meteorological disaster risk assessment, Zhang et al. (2021) evaluated the heat hazard for summer maize in the Haihe Plain by describing the severity of extreme heat events through the continuous days and cumulative temperature. Danjun et al. (2017) used the spatial vegetation drought index (SVDI) combined with probability density curves to assess the drought hazard in west-central Jilin Province.

Although, as the global environment changes, scientists are gradually recognizing the neglect of the field of CEEs research (Damalas et al., 2018; Lee et al., 2020; Wang et al., 2020). Most studies have also focused on one extreme event or described probability, duration, or intensity in isolation. In addition, in studies of CEEs, due to confusion between the concepts of hazard and risk, the evaluation of crop hazard often typically ignores the association between probability and severity. This might lead to considerable uncertainty in the subsequent risk assessment. In this regard, it becomes more urgent to construct a hazard assessment model for CEEs and to rapidly assess the hazard of CEEs in real-time.

In this study, we used maize as an object of study to construct DHCEEs hazard assessment model., combining the magnitude index and the copula function, so that the model can simultaneously consider the severity, duration, and probability of occurrence of the DHCEEs. The study allowed: (1) Analysis of multi-year changes in drought and heat conditions during different growing periods of maize. (2) Understanding the occurrence of DHCEEs in maize in the Songliao Plain. (3) To construct a DHCEEs hazard assessment model and obtain the characteristics of DHCEEs hazards. The model will be applied to the Songliao Plain, which is known as the golden corn belt in northern China. This research result can help to understand the characteristics and patterns of agro-meteorological disaster occurrence in-depth, and is a further exploration of the comprehensive assessment of the risk of CEEs, increasing the accuracy and relevance of risk assessment.

2. Study area and data

2.1. Study areas

Songliao Plain (SLP: 118°40′E to 128°00′E to 40°25′N to 48°40′N) is located in northeast China, it covers southern Heilongjiang Province, central and western Jilin Province, and most of Liaoning Province (Fig. 1) (Bin et al., 2020; Ting-ting et al., 2014). It envelops an all-out area of around 3×10^5 hm^2. Maize is one of the principal crops planted in Songliao Plain, representing around 1/3 of the national total output, 1/4 of the total sown area, and more than 1/2 of the total export volume (Guo et al., 2022). The yearly precipitation in the review region is 500–750 mm and the yearly mean evaporation is 2–3 times that of the yearly mean precipitation (Guna et al., 2019). The highest temperature occurs in July and August. Farming relies essentially on rainfall. Irrigation and fertilization methods are single(Zhang and Hayakawa, 1999). As of late, the occurrence of extreme heat and the increase of drought events have brought more uncertainty to maize production.

2.2. Data source

Investigation of the effect of complex interaction between land and atmosphere requires long-term observation of basic hydrological variables, such as soil moisture, precipitation, and evaporation from the land surface (or "evapotranspiration"). The Global Land Evaporation Amsterdam Model (GLEAM) has four fundamental modules (Potential

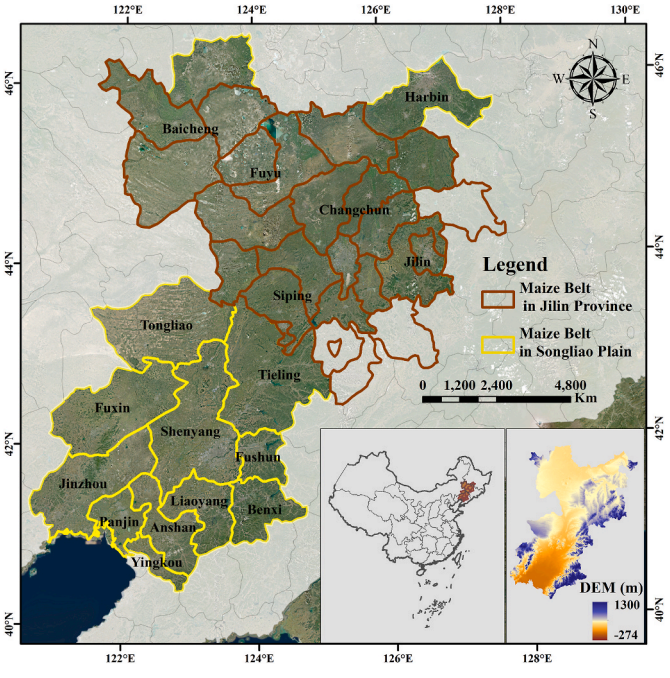

Fig. 1. Sketch map of the study area.

evaporation module, Rainfall interception model, Soil module, Stress module), which is a set of algorithms specially used to estimate land evaporation and soil moisture in root zone from satellite data (Martens et al., 2017; Miralles et al., 2011). We obtained daily data on root-zone soil moisture (SMroot: 10–100 cm) and surface soil moisture (SMsurf: 0–10 cm) from GLEAM from 1990 to 2020. Datasets are provided on a 0.25° × 0.25° latitude-longitude grid, with a daily temporal resolution.

The temperature data comes from the China Global Land Reanalysis System (CMA-RA) established by the National Meteorological Information Center with the core technologies of ensemble assimilation algorithm, multi-source fusion method, Noah 3.3 land surface model, and surface parameter optimization (http://data.cma.cn/). Datasets are provided on a 0.5° × 0.5° latitude-longitude grid, with a 3 h temporal resolution. We use bilinear interpolation technology in ArcGIS to reduce the data to 0.25° × 0.25° spatial scale.

We collected maize yield and growth period data for 31 prefecture-level cities in the Songliao Plain from 1990 to 2020. The data are mainly obtained from provincial statistical yearbooks, Weather Bureau, and Statistical Bureau. The quadratic exponential smoothing method was used to detrend the yield data. According to the actual growth records of maize in the study area, the growing period was divided into April (Seeding); May (Seedling - Three-leaf stage); June (Three-leaf - Jointing stage); July (Jointing - Silking stage); August (Silking - Milk stage); September (Milk -Mature stage). The food crops planting area and the drought covered area are from the National Bureau of Statistics (http://www.stats.gov.cn/tjsj/). The standard geographical information data came from the National Catalogue Service for Geographic Information website (http://www.webmap.cn).

3. Method

The general flowchart of this research is presented in Fig. 2. The following sections describe the steps in detail.

3.1. Soil moisture deficit index (SMDI)

SMDI is an agricultural drought index put forward by Narasimhan and Srinivasan in 2005 (Narasimhan and Srinivasan, 2005). SMDI is not affected by climate types and seasons, which is suitable for describing short-term drought conditions and has good spatial comparability. At present, it is widely accepted and applied in agricultural drought research (Narasimhan and Srinivasan, 2005). In this study, GLEAM daily grid data of 0–100 cm soil layer from 1990 to 2020 are used for calculation:

$$SMDI_j = 0.5SMDI_{j-1} + \frac{SD_j}{50} \tag{1}$$

Where SD_j is soil moisture deficit or excess (%) and can be computed as:

$$SD_{i,j} = \frac{SW_{i,j} - MSW_j}{MSW_j - minSW_j} \times 100, if SW_{i,j} < MSW_j \tag{2}$$

$$SD_{i,j} = \frac{SW_{i,j} - MSW_j}{maxSW_j - MSW_j} \times 100, if SW_{i,j} > MSW_j \tag{3}$$

Where $SW_{i,j}$ is the soil moisture for the i day and the j grid (m^3/m^3). MSW_j is the median of long-term soil moisture. $MaxSW_j$ and $minSW_j$ are the long-term maximum and minimum soil moisture, respectively. The scope of the $SMDI$ esteem shifts from −4 to 4, showing extreme dry to extreme wet circumstances.

3.2. Temperature condition index (TCI)

Before determining the degree of heat events, it is necessary to construct an index that can reflect the influence of temperature. TCI can more conveniently identify heat events and calculate the intensity, and can also achieve spatial comparability.

$$TCI_{i,j} = \frac{T_{i,j} - T_{min,j}}{T_{max,j} - T_{min,j}} \tag{4}$$

Where $T_{i,j}$ is the average temperature from 12 noon to 3 p.m. for the ith

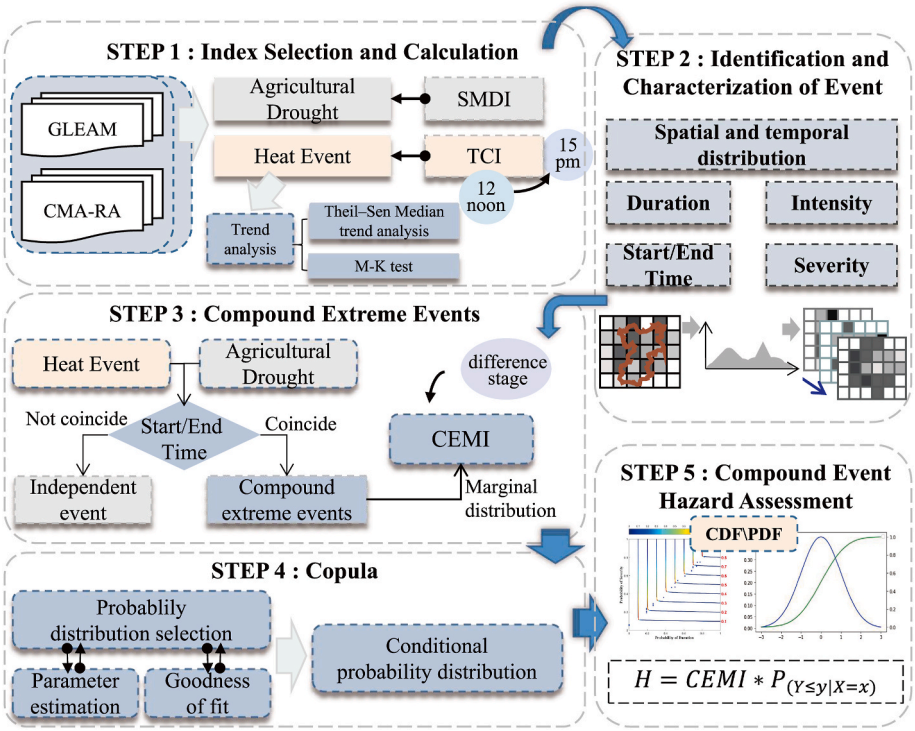

Fig. 2. The methodological framework of this study.

day and the jth grid (°C). $T_{min,j}$ and $T_{max,j}$ represent the lowest and highest temperatures from 1990 to 2020 respectively. The value of *TCI* is between [0–1]. The higher the temperature, the value of $T_{i,j}$ is close to $T_{max,j,}$ and the value of *TCI* is close to 1, otherwise, it is close to 0.

The heat stress index is based on the extremely high temperature threshold in the growth stage of maize. When the temperature exceeds the threshold, morphological markers such as pollen vitality, stamen growth, and interval between flowering and silking will be affected (Lizaso et al., 2018; Lyakh et al., 1991). When heat occurs in the critical period of determining grain numbers, it will lead to a huge drop in yield. The heat threshold widely recognized by researchers is 30–33 °C from Seedling to Jointing stage, 30–35 °C from Jointing stage to Milk stage, 30–35 °C from Milk stage to Mature stage (Xin-ying et al., 2021; Zhang et al., 2020). Different researches on extreme events have different understandings and definitions. Extreme events may be different from normal conditions (Abnormal), or they may be different from what the carrier needs or can accept (Stressful). Combined with the abnormal and stressful, and considering the actual perceived temperature, 30 °C was selected as the heat threshold of maize in this study. The data is the daily average temperature of 3 h (12 noon-15 p.m.). This kind of data reflects that maize is affected by the lowest 3-h heat every day and the heat event lasts for several days.

3.3. Theil - Sen median trend analysis and the Mann - Kendall test

Theil-Sen Median method is a robust trend calculation method for nonparametric statistics. Mann-Kendall is a nonparametric statistical test method used to determine the visibility of trends. The common points of the two methods are as follows: (1) the data are not required to obey a specific distribution; (2) Strong resistance to data outliers. (3) High computational efficiency and insensitivity to measurement errors and outliers (Dinpashoh et al., 2014; Jiang et al., 2015; Serrano-Notivoli et al., 2018).

$$\beta = mean\left(\frac{x_j - x_i}{j - i}\right), \forall j > i \tag{5}$$

Where x_i and x_j are time-series data of grid cells. $\beta > 0$ indicates that the time series shows an upward trend; $\beta < 0$ indicates a downward trend.

$$S = \sum_{i=1}^{n-1} \sum_{j=i+1}^{n} sign\left(x_j - x_i\right) \tag{6}$$

$$\theta = x_j - x_i \tag{7}$$

$$sign(\theta) = \begin{cases} 1 & \theta > 0 \\ 0 & \theta = 0 \\ -1 & \theta < 0 \end{cases} \tag{8}$$

$$E(s) = 0 \tag{9}$$

$$Var(s) = \frac{n(n+1)(2n+5)}{18} \tag{10}$$

$$Z = \begin{cases} \dfrac{S-1}{\sqrt{Var(S)}} & S > 0 \\ 0 & S = 0 \\ \dfrac{S+1}{\sqrt{Var(S)}} & S < 0 \end{cases} \tag{11}$$

Where n is the number of days. When the absolute value of z is greater than 1.65, 1.96, and 2.58, the indicated trend has passed the significance test with the reliability of 90%, 95%, and 99% respectively (Table 1).

Table 1
Theil - Sen Median trend analysis and the Mann - Kendall test trend categories.

β	Z	Trend type	Trend features
$\beta > 0$	$2.58 < Z$	4	Very significant increase
	$1.96 < Z \leq 2.58$	3	Significant increase
	$1.65 < Z \leq 1.96$	2	Slight significant increase
	$Z \leq 1.65$	1	Non-significant increase
$\beta > 0$	Z	0	Unchanged
$\beta > 0$	$Z \leq 1.65$	−1	Non-significant decrease
	$1.65 < Z \leq 1.96$	−2	Slight significant decrease
	$1.96 < Z \leq 2.58$	−3	Significant decrease
	$2.58 < Z$	−4	Very significant decrease

3.4. Define extreme events and compound extreme events

Because one of the characteristics of stress events is related to the spatial component, the soil moisture and temperature data are resampled to the Asia North Albers Equal Area Conic with the resolution of $0.25° \times 0.25°$.

3.4.1. Events characteristics

In this study, it is defined that the drought event starts at SMDI ≤ -2 and ends at SMDI > -2. The VCI value of each grid is obtained by calculating the maximum and minimum temperature of each grid, and the VCI threshold of each grid is calculated by taking 30 °C as the threshold. When temperature is higher than threshold, a heat event begins, and when it is lower than this, the event ends. Another consideration in the selection of threshold is to obtain a relatively large number of compound event records. If the time interval between two adjacent events is one day, it will be merged into one heat or drought event, and the disaster event with the disaster event length of one will be excluded. When the drought event and the heat event coincide in time in the same grid, it is recorded as a compound event.

(1) Duration: The duration of drought events, heat events, and DHCEEs, that is, events are the time interval between the start (ts) and the end (te) of events in the grid. The duration of the DHCEEs is based on the one that takes a long time among the drought and heat events.
(2) Severity: It is an expression of the severity of the incident. It reflects the degree to which crops are affected by specific drought and heat events. Calculate the cumulative sum of the difference between the indicator and the indicator threshold.

$$S_{SMDI} = \sum_{t=ts}^{te} (SMDI_i - SMDI_{th}) \tag{12}$$

$$S_{TCI} = \sum_{t=ts}^{te} (TCI_i - TCI_{th}) \tag{13}$$

Where S_{SMDI} and S_{TCI} are the severity of drought and heat events, *ts* and *te* are start time and end time of events, $SMDI_i$ and TCI_i are drought and heat index values of each grid point, and $SMDI_{th}$ and TCI_{th} are event thresholds.

(3) Intensity: It is the average of the severity of the event, which represents the intensity of the event's development.

$$I_{SMDI} = \frac{\sum_{ts}^{te+1} SMDI}{(ts - te + 1)} \tag{14}$$

$$I_{TCI} = \frac{\sum_{ts}^{te+1} TCI}{(ts - te + 1)} \tag{15}$$

Where I_{SMDI} and I_{TCI} are the intensity of drought and heat events.

3.4.2. Compound event magnitude index (CEMI)

Compound event magnitude index is a good method to combine heat and drought events and eliminate the difference between units and magnitudes (Wang et al., 2021; Wu et al., 2019). After identifying the compound events, the index is converted into non-exceedance probability by fitting the marginal distribution function (Fig. 3). In this study, the severity and intensity values calculated by the drought index are multiplied by a constant (−1) to become positive numbers to facilitate calculation. The calculation formula is as follows:

$$CEMI = P_{SMDI}(S_{SMDI}) * P_T(S_{TCI}) \tag{16}$$

Where P_{SMDI} and P_T are the non-exceedance probability of drought and heat, respectively, which fall within [0,1], with large S_{SMDI} and S_{TCI} corresponding to high probabilities. Detailed description of these methods is referred to Wu et al. (2019).

3.5. Copula

Copula function is a multidimensional joint distribution function defined in [0,1] uniform distribution, and its construction does not need to consider the marginal distribution (Salvadori and De Michele, 2004, 2010). The appearance of copula provides an effective method to describe various characteristics of compound events. Let X and Y be continuous random variables, and their marginal distribution functions are FX(x) and FY(y) individually, and the joint distribution function is F (x, y) (Salvadori et al., 2011, 2013). If each marginal distribution functions are continuous, there is a unique function copula function C (u, v), which makes:

$$F(x,y) = C\left[F_x(x), F_y(y)\right] = C(u,v) \tag{17}$$

$$f(x,y) = c(u,v) f_X(x) f_Y(y) \tag{18}$$

Where, *F(x, y)* is the joint distribution function; C represents the Copula Function. *u=FX(x)* and *v=FY(y)* are marginal distribution functions of random variables X and Y, respectively. c(u, v) is the density function of Copula. $f_X(x)$ and $f_Y(y)$ are the probability density functions of random variables *X* and *Y*, respectively.

The construction of the copula function can be divided into three processes: (1) Construct the marginal distribution of random variables; (2) Fit of copula function; (3)Test of copula function. The Spearman coefficient is used to measure the correlation between variables. In this study, 17 theoretical distributions were employed to fit the univariate probability distributions (Table SI. 1). The best marginal is chosen by BIC value. Eight copula functions are mainly selected in the construction of the joint probability distribution function (Table SI. 2). Markov chain Monte Carlo simulation was utilized to work out the parameters included in the copula function under the Bayesian framework. Akaike Information Criterion (AIC), Bayesian Information Criterion (BIC), and Root Mean Squared Error (RMSE) are used as performance metrics to judge the goodness of fit of the copula function. Detailed description of these methods is referred to Sadegh et al. (2017).

When the severity value of the compound event is $CEMI_i$, the duration of the compound event may be arbitrary, and the probability of occurrence of different durations is different. Conditional distribution can be used to predict the probability under such circumstances (Sadegh et al., 2017). Derived from copula function, when (X, Y) is a two-dimensional continuous random variable, its probability density function is. For a fixed x value (duration) (Aas et al., 2009), there are:

$$f_{Y|X}(y) = \frac{f(x,y)}{f_X(x)} = \frac{c(u,v) f_X(x) f_Y(y)}{f_X(x)} = c(u,v) f_Y(y) \tag{19}$$

The conditional distribution function under the condition of X = x is as follows:

$$F_{Y|X}(y) = P(Y \le y | X = x) = \frac{\partial F(x,y)/\partial x}{dF_X(x)/dx} = \frac{\partial C(u,v)}{\partial u} \tag{20}$$

$f_Y(y)$ and $f_X(x)$ represent the probability density functions of random variables *X* and *Y*, respectively. As long as the joint distribution function of *X* and *Y* is known, the conditional probability distribution function $F_{Y|X}(y)$ can be deduced. *C(u,v)* is copula function, and *c(u,v)* is the corresponding probability density function.

3.6. Compound extreme Event hazard assessment model

Hazard assessment is the first step of disaster risk assessment, which mainly measures the disaster intensity of disaster-inducing factors to disaster-bearing body. Meteorological hazard refers to the degree of variation of meteorological factors that can cause disasters. Multi-hazard evaluations for multiple extreme events should include two components (1) different extreme events that threaten the same exposed elements (with or without temporal coincidence); and (2) extreme events that occur simultaneously. Based on the regional disaster system theory and the formation mechanism of comprehensive risk of agro-meteorological disasters, this study considers that the hazard is mainly determined by the probability of disasters and the severity of disasters (Cui et al., 2021). Generally, events with high frequency and severity are at greater hazard.

$$H = CEMI \times P_{(Y \le y_1, x_{CEMI})} \tag{21}$$

Where *H* is the hazard of compound events, and *P* represents the probability of compound events with severity x_{CEMI} and duration less than or equal to y_1. *Y* is compound event duration days. Copula is used to estimate the probability of compound events.

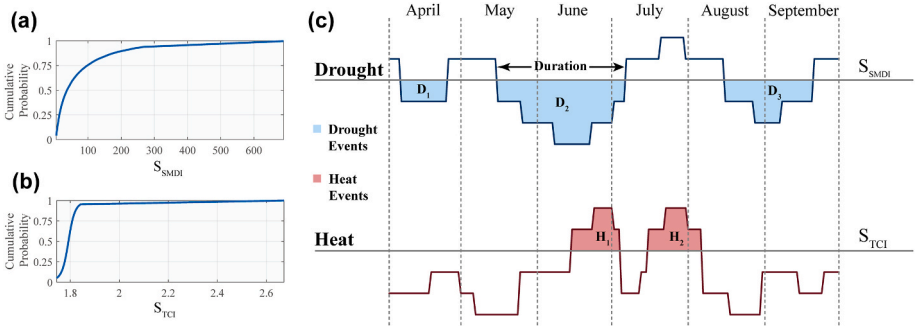

Fig. 3. CEMI illustration based on SMDI and TCI. (a) and (b) are cumulative probability curves of SSMDI and STCI, separately. (c) The gray line is the threshold value of drought and heat index. The blue area represents drought events, and the red area represents heat events. (For interpretation of the references to colour in this figure legend, the reader is referred to the Web version of this article.)

4. Results

4.1. Spatio-temporal distribution characteristics of extreme events

In this section, the Theil-Sen Median trend analysis and Mann-Kendall test are respectively used to test the development trend and significance of SMDI and TCI in different growth periods of maize from 1990 to 2020 (Fig. 4). The warming trend was most significant in the southeastern part of the study area (Fig. 4 (a1-a6)), and the most significant increases were concentrated in June, July, and August. In July (Fig. 4 (a4)), the area of significant and very significant areas accounted for 49.83% of the total area, mainly concentrated in the eastern and southern parts and a small part of the northwestern part, while the slight significant area accounted for 12.22%. In August (Fig. 4 (a5)), 0.96% of the regions had a very significant increase in the TCI, 10.29% had a significant increase, and 9.00% had a slight significant increase. The areas of significant increase are concentrated in the northeast corner, south, and northwest corner. A significant increasing trend of TCI (very significant, significant, slight significant) was observed in the southeast direction in June with 21.54% of the regions (Fig. 4 (a3)). Beyond, there is a tendency for the occurrence of low temperatures to increase in the context of climate change (Fig. 4 (a1, a2)). The regions with significantly lower TCI (very significant, significant, slight significant) in April, May, and September represent 30.23%, 36.33%, and 2.89% of the total regions, respectively (Fig. 4 (a1, a2, a6)).

SMDI is generally increasing in the Northeast, while it is trending downward in the Southeast and Northwest (Fig. 4 (b1-b6)). Soil moisture in the southeastern part of the study area was continuously tilting toward a deficit state, showing a significant decreasing trend. Among them, 15.76%, 4.50%, 7.72%, 7.72%, 31.19%, and 4.82% of the total area of the study area with significant decrease (very significant, significant, slight significant) agricultural drought from April to mid-September, respectively. The SMDI in the northeastern part of the Songliao Plain (southeastern Jilin Province) tends to increase from an overall perspective because it is mountainous and belongs to the semi-humid-humid zone.

4.2. Identification and characterization of extreme events

In this study, the number of events, duration, severity, and intensity of all drought and heat events occurring in each grid from 1990 to 2020 were identified separately by applying the runs theory (Fig. 5). In terms of the number of events, the number of events in the southern region (Jinzhou, Panjin, Fuxin, Yingkou, and Anshan) ranged from 50 to 73, about 2 events per year. This was followed by the northwest region (Baicheng and Fuyu) and the northeast region (Harbin), where the number of events averaged over 40 (Fig. 5 a1). Heat events were frequent in the northwestern and southern parts of the study area. The number of events ranged from about 11 to 26.9 (Fig. 5 a2). Judging from the duration of the event (Fig. 5 (b1, b2)), the longest drought events are concentrated in the north, lasting for 183 days, which is equivalent to the whole growth period under drought stress. The shortest was 2 days. Long-lasting heat events are mainly concentrated in the southwest and northwest regions, with the longest duration of 13 days and the shortest duration of 2 days. The analysis of event severity and intensity can control and analyze the event from the perspective of cumulative intensity and degree (Fig. 5 (c1, c2, d1, d2)). Areas with higher severity or intensity were similar in distribution to areas with longer duration of events, whether heat or drought.

Separate analysis of severity and intensity can capture the events in terms of cumulative intensity and degree. Areas with higher severity or intensity are similarly distributed to areas with longer event durations, whether they are heat events or drought events. Some events were found to be small in severity but large in intensity and small in duration, which is consistent with the characteristics of flash drought and rapid warming and needs further analysis. Statistics on the main characteristics of drought and heat events in the Songliao Plain revealed (Table 2) that, in terms of drought events, the duration has been increasing, while the severity and intensity of droughts have generally increased. The years 2001–2004,2008,2015, and 2017 all experienced drought events that lasted throughout the maize growth period. Drought events affecting more than 50% of the total area of the study area occurred in 15 of the 31 years. The severity and intensity of heat events increased, with an average impact area of 6% of the total area (15,114.6 km^2).

4.3. Identification of compound extreme events

Seventeen theoretical distributions were selected to fit the characteristics of drought and heat events within each grid. The marginal distribution of drought severity is Birnbaum-Saunders , Exponential , Generalized Pareto (gp) , and Inverse Gaussian distribution, and heat severity is generalized extreme value (gev) and gp. The Chi-square test

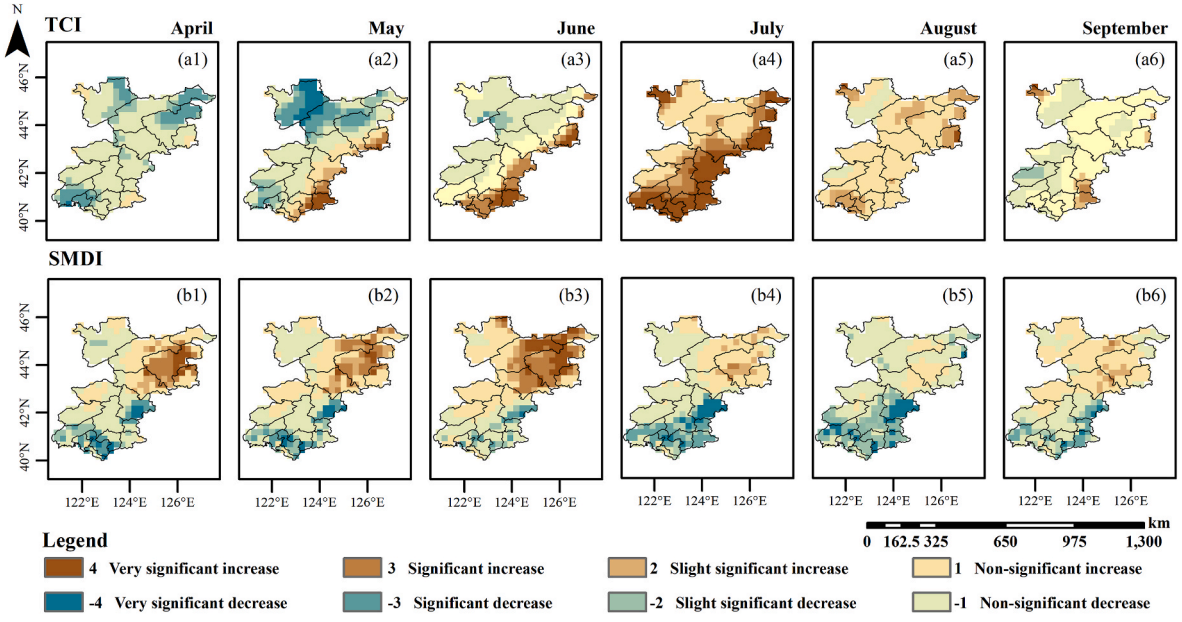

Fig. 4. Spatial distribution of trends and significance of TCI (a1 - a6) and SMDI (b1 - b6) in the study area from 1990 to 2020.

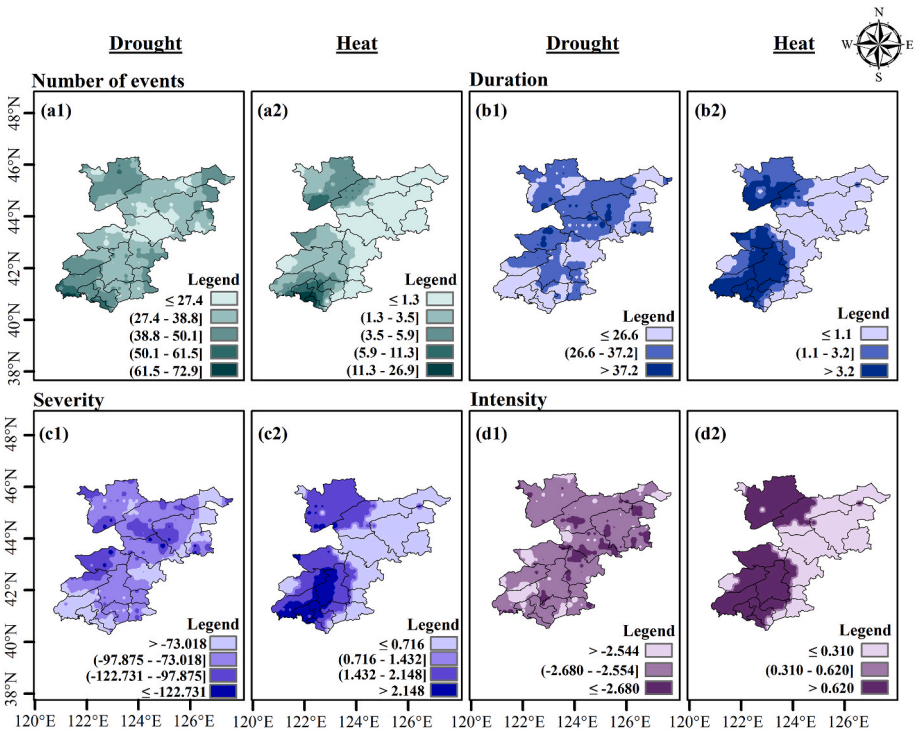

Fig. 5. Spatial distribution map of the number of events (a1, a2), duration (b1, b2), severity (c1, c2), and intensity (d1, d2) of drought and heat events in the study area from 1990 to 2020. (a1, b1, c1, d1 are drought event characteristics. a2, b2, c2, and d2 are heat event characteristics.)

Table 2
Statistics of drought and heat events characteristics.

Evens characteristics		Drought Evens			Heat Evens		
		1990–2000	2001–2010	2011–2020	1990–2000	2001–2010	2011–2020
Duration (d)	Mean	23	30	27	2	3	3
	Max	155	183	183	6	9	13
	Min	2	2	3	2	2	2
Severity	Mean	−67.17	−91.39	−81.28	1.96	2.08	2.23
	Max	−517.45	−724.56	−706.58	5.35	8.19	11.38
	Min	−4.00	−4.00	−4.00	1.74	1.74	1.75
Intensity	Mean	−2.56	−2.64	−2.61	0.89	0.90	0.92
	Max	−3.95	−3.99	−3.97	0.94	0.95	0.96
	Min	−2.00	−2.00	−2.00	0.88	0.88	0.88
Average area (km^2)		104180.73	173502.00	101331.00	10935.98	18792.51	15876.00

was used to estimate the parameters of the marginal distribution function. The Kolmogorov - Smirnov method was used to evaluate the GOF. All optimal distributions passed the $\alpha = 0.05$ significance test. The CEMI obtained by the marginal distribution function of SMDI and TCI can reflect the intensity of DHCEEs and takes into account the effect of the event duration on the event intensity. CEMI was significantly and positively correlated with heat duration, drought duration, heat severity, and heat intensity. It is significantly negatively correlated with drought severity and drought intensity, which is due to the negative value of the drought index. (Fig. 6).

The spatial distribution of the mean CEMI values of DHCEEs in the study area was plotted for the selected years 1997,2001,2016 and 2018 (Fig. 7). In 1997 (Fig. 7a), DHCEEs occurred in the northwestern part of the study area, with Zhenlai, Da'an, Qianguo, and Qian'an being more serious, with DHCEEs concentrated in June and July. In 2001 (Fig. 7b), CEMI was concentrated in Zhenlai, Da'an, Qianan, Changling, Qianguo, and Tongyu, the intensity is similar to 1997, concentrated in July and August. In 2016 (Fig. 7c), the scope of DHCEEs decreased, the intensity of the impact was reduced, and the affected areas were Taonan, southern Zhenlai, and Da'an, concentrated in August. The 2018 DHCEEs were concentrated in July and August in southern Liaoning (Fig. 7d). According to the statistics of all DHCEEs in the Songliao Plain from 1990 to 2020, it was found that DHCEEs are mainly located in Anshan, Baicheng, Fuyu, Fuxin, Jinzhou, Panjin, Shenyang, Siping, Tongliao, Yingkou, and Changchun. The months of occurrence are concentrated in July and August, which are the jointing - silking stage and silking - milk stage of maize.

4.4. Compound event hazard assessment

In this section, the hazard of DHCEEs in 1997, 2001, 2016, and 2018 is calculated using the compound events identified in section 2.5 and the hazard assessment model constructed in section 2.6 combined with the copula. The optimal marginal distribution functions for CEMI and compound events duration were beta and gp, respectively. the optimal copula functions were Gaussian copula (RMSE = 0.5056 , NSE = 0.9797). From the results, the most severe compound event hazard in 1997 (Fig. 8a), 2001 (Fig. 8b), and 2016 (Fig. 8c) were located in the northwestern part of the study area. In 2018 (Fig. 8d), the DHCEEs moved to the south and increased in intensity. The hazard in 2016 was the lowest in four years, which may be related to the compounded event characteristics of high heat severity and low drought severity in that

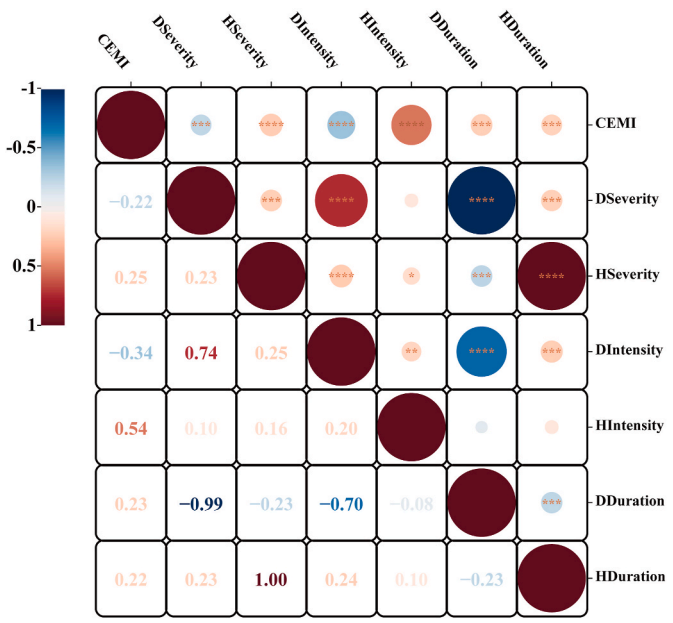

Fig. 6. Heat map of correlation between CEMI and severity, intensity, and duration of drought, and heat events. HSeverity and DSeverity are the severity of heat and drought events, respectively; HIntensity and DIntensity are the intensity of heat and drought events; HDuration and DDuration are the duration of heat and drought events ****, ***, **, and * indicate $p < 0.001$, $p < 0.01$, $p < 0.05$ and $p < 0.10$, respectively.

year. Combined with Fig. 5, the heat events and drought events with higher severity and intensity occurred in the northwestern and southwestern parts of the study area, and the eastern part was not as severe as the western part. Fig. 9 shows the conditional cumulative probability curves under different CMEI scenarios. The four situations have similar patterns. With the increase of CEMI, the probability of compound events decreases. For example, for an event with a duration of 6 days, with the CEMI increased from 0.25 to 0.5, 0.75, and 0.9, the probability of occurrence decreases by 2.7%, 4.2%, and 5.0% respectively.

5. Discussion and conclusion

5.1. Discussion

The occurrence of an extreme event or even a disaster may be an extreme state of a single meteorological factor, however, it is more likely to be a composite effect of multiple interdependent extreme events. Most studies on CEEs tend to analyze one of these events in isolation, ignoring the temporal and spatial overlap of the events and their persistent

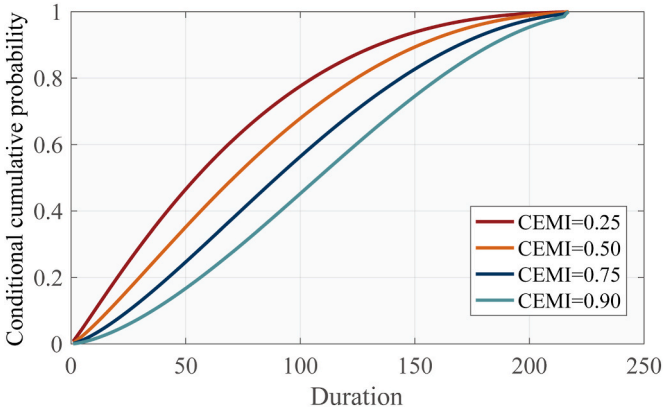

Fig. 9. Conditional cumulative probability distributions for different compound event intensities.

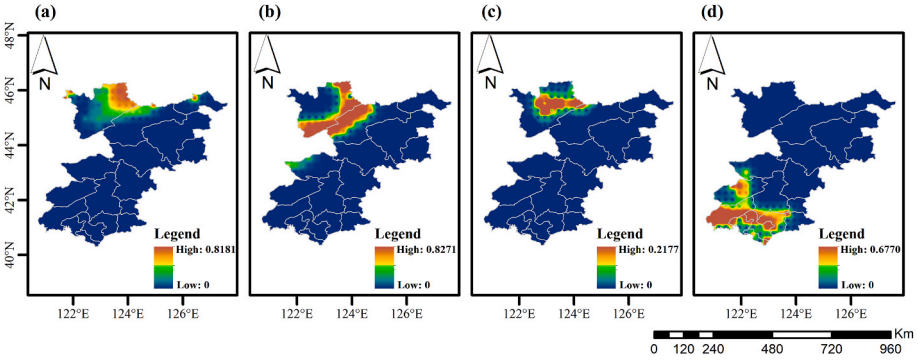

Fig. 7. Magnitude of compound drought and heat events in typical years in Songliao Plain. (a: 1997; b: 2000; c: 2016; d: 2018) .

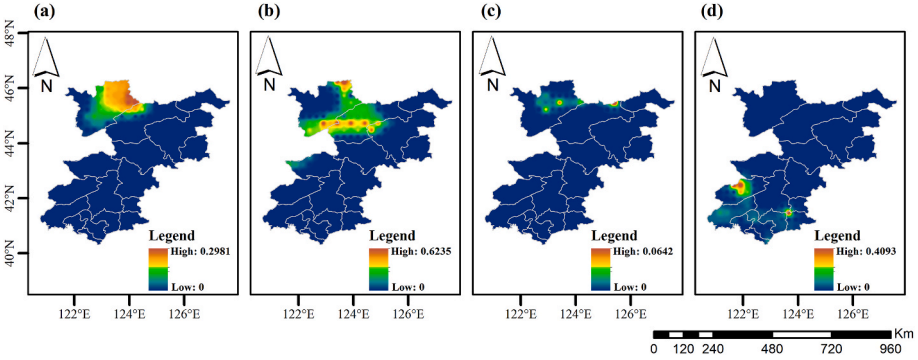

Fig. 8. Hazard assessment of compound drought and heat events in typical years in Songliao Plain.

characteristics. Our study establishes a hazard assessment model for DHCEEs based on regional disaster system theory and agro-meteorological disaster risk assessment theory, combining magnitude index and copula function, which takes into account the severity, duration, and probability of occurrence of the CEEs. Allows for comprehensive consideration of the developmental stages of the events and real-time assessment of their risk. It helps to increase the accuracy and relevance of risk assessment and better guide the formulation of risk management and disaster mitigation countermeasures for agricultural production.

5.1.1. DHCEEs affect the growth and development of maize

In the context of global warming, temperatures are generally rising in China (Li et al., 2022). The heat events in the study area mainly occurred from mid-June to mid-August, with the most frequent occurrence from late July to mid-August (200–240). At this time, maize grown will be going through important stages such as jointing, teaselling, flowering, silking and grain filling stage. Drought during the jointing stage of maize will lead to hindered differentiation of the female ears, affecting the normal growth and development of filaments and forming empty poles or ears. Heat at the jointing stage will affect the synthesis and transport of organic matter in maize plants and the differentiation of male and female ears. The DHCEEs at this time mainly affect maize kernel plumpness. The main causes of yield reduction due to drought during the tasseling-silking stage were the decrease in ear length and grain number, the shortened flowering stage, and the decrease in pollen activity. At this time, heat will lead to obstruction of pollen dispersal and further decrease of pollen quantity and activity (Ayub et al., 2021; Hussain et al., 2019; Lizaso et al., 2018; Siebers et al., 2017; Wilhelm et al., 1999). Temperature during the filling stage is the main factor affecting photosynthesis and substance reaction enzyme activity. Extreme heat events can cause disturbance in the output and distribution of photosynthetic products. It also accelerates leaf senescence and reduces dry matter accumulation and nutrient formation. Heat and drought directly affect the rate of grain filling when they occur together. Rapid dehydration of the grain is accompanied by the phenomenon of heat forcing maturity. Therefore, DHCEEs during the filling stage pose a significant threat to both yield and seed quality (Sánchez et al., 2014; Wang et al., 2022; Zhu et al., 2018, 2019).

We analyzed the growth period of maize. Only the silking stage showed a slight tendency to advance (Figure SI. 1). We believe that the delay of the seeding date is related to the northward expansion of middle and late maturity maize varieties, mainly concentrated in southwest Heilongjiang and northern Jilin. This part is also an area where drought events and heat events occur severely (Fig. 4). And the sowing and emergence stages of most sites in west-central Jilin Province and Liaoning Province showed an early trend. Changes in climatic resources affect maize phenology, and changes in phenology also reflect climate change to some extent. The maize growth period in the study area was extended at the seedling - three-leaf stage, silking - milk stage, and milk-mature stage. The middle and late growth period of maize in most sites in the study area is prolonged, which will expose more to heat (Figure SI. 2).

The variation in the length of the growth period is mainly related to climatic factors and maize varieties. For example, in terms of varieties, late maturing varieties had a long filling stage and relatively low filling rate, while early maturing varieties had a short filling stage and relatively high filling rate. The selection of late maturing varieties is more conducive to offset the shortening of the filling stage due to heat. In terms of climate factors, the relatively large annual temperature fluctuations in the northern region also lead to a large variation in the cumulative temperature required for each growth period of maize from year to year, and the variation in the growth period is more unstable (Huo et al., 2023). Combined with the analysis of previous research results, we believe that appropriate temperature increase may positively affect yield and grain quality by affecting the length of maize growth periods. However, in the context of increasing heat and drought stress, it is uncertain whether this kind of increase in maize yield can offset yield losses in previous stages (Minoli et al., 2022; Zhu et al., 2018, 2019). Risk assessment and management research in this area needs to be further explored.

July and August is the month with the most significant warming trend in the Songliao Plain, which corresponds to the jointing - silking stage of maize, when maize is most sensitive to temperature (Hussain et al., 2019; Mayer et al., 2014; Qaseem et al., 2019).In addition, drought events were more scattered, characterized by long duration, wide impact, and high intensity (Li et al., 2015; Ye et al., 2019; Yue et al., 2018). The more severe heat events were concentrated in the northwest and southwest. The areas where the more severe compound extreme events occurred roughly overlapped with the areas where heat occurred. The data from the correlation analysis showed a positive correlation between CEMI index and heat intensity ($p < 0.001$). In the future, there is a trend of further temperature increase in the study area, while most of the land areas will experience severe and widespread drought (Dai, 2013). This makes the coincidence of heat and drought around the flowering stage of maize likely to be a major limiting factor for maize production in the Songliao Plain.

5.1.2. Yield decreased linked to DHCEEs

According to previous studies and records of the disaster canon, 1997 was a typical drought disaster year in Jilin Province, and grain production decreased by about 20% due to drought (Jia et al., 2018). 2001 was a typical major drought year in Northeast China, and the ratio of drought disaster area to total disaster area was greater than 80% (Li and Lyu, 2022), while 2001 was the 4th highest temperature year in Jilin Province for the same period since the founding of the country (Xi, 2001). 2018 was a typical heat and drought year in Liaoning Province (Min et al., 2019). To confirm the reasonableness of the hazard evaluation results, we reverse analyzed the occurrence of extreme events in years of reduced maize production. The calculation method of yield reduction rate and the classification of the year's harvest in yield are shown in China Meteorological Industry Standard QX/T335-2016. Table SI. 3 shows the years in which different levels of yield reduction in maize occurred and the years in which the typical DHCEEs identified in this study occurred. Typical year is defined as the year in which the hazard calculation results are in the first 50% of the years of the DHCEEs. In the year of maize production reduction, the frequency of DHCEEs is higher (Figure SI. 1). This is consistent with the calculation of the CEMI index. Ari guna calculated the spatial distribution of maize yield reduction rate in the Songliao Plain from 1981 to 2018, and its results also showed that the level of yield reduction rate in the southwestern (Jinzhou, Panjin, Anshan, Liaoyang, Fuxin) and northwestern (Baicheng, Songyuan) parts of the Songliao Plain was relatively high (Ari et al., 2021). In general, there are cases where yield reductions are not related to DHCEEs. However, yield reductions occurred more frequently in years of high hazard than in other years. This indicates that the constructed hazard assessment model better reflects the situation of maize DHCEEs in the study area.

Frequent heat events are generally of low intensity and are often recorded together with drought events. Overall, we believe that heat events do exist in the northeast, but there has not been a long-term large-scale significant warming that has rarely had a serious impact on corn production alone. However, the risk of compound events in the southwestern part of the study area tends to increase after 2015, probably due to the relatively high number of heat events and significant warming trend in the region, and the increased probability of compounding with drought events.

There are several points to note about our study. First, our study provides an evaluation model that can calculate the risk of compound events dynamically in real time. However, the simultaneous occurrence of heat and drought is only one model for the occurrence of compound extreme events. The correspondence between meteorological factors

and crops is more complex. Second, we takes into account both intensity, duration, and frequency, but assumes a grid for the range of occurrence of a single event, which may neglect the hazard at times when the range of occurrence is wide but the intensity is low. Adding the factor of event occurrence range can increase the accuracy of event intensity. Also, we plan to further explore the similarities and differences between the effects of heat on crops in days and in hours.

The hazard evaluation model established in this paper combines the magnitude index and the copula model, which can take into account the intensity and probability of the composite event at the same time and can show the hazard level of the event better than the simple recurrence period calculation and occurrence probability calculation. By constructing a joint distribution, the hazard of a compound event can be evaluated in real time. By combining real-time monitoring and early warning information, we can quantify the risk of crop hazards in a specific warning area in real time, so as to better guide agricultural production and layout.

5.2. Conclusion

In this study, the comprehensive index CEMI of compound extreme events of drought and heat was constructed by using SMDI index and TCI index, and the risk evaluation model of compound extreme events was constructed by combining copula function. The severity was determined by the cumulative distribution function of drought events and heat events, respectively. The fitted probability of a specific compound extreme events is obtained from the conditional distribution probability calculus constructed by the copula formula. The main findings are as follows:

(1) July was the most significant warming trend in the study area, and the increase in drought was most severe in July and August. The northwestern and southwestern regions are the areas where heat events occur with relatively high intensity and severity. Drought events, on the other hand, affect the entire region of the Songliao Plain with varying degrees of severity.
(2) The result of CEMI is reliable. CEMI was significantly correlated with the duration, severity, and intensity of drought and heat, with the largest correlation coefficient with the intensity of heat, $p < 0.001$. high CMEI values were mainly found in northwest and southwest regions.
(3) Events of high intensity have a lower probability of occurrence compared to events of low intensity, but may have similar hazards, which can be well quantified by the hazard assessment model constructed in this study. Hazardous less than 0.1 of the event accounted for 46.51%; greater than 0.1 less than 0.2 accounted for 17.83%; greater than 0.2 less than 0.3 accounted for 18.60%; greater than 0.3 less than 0.4 accounted for 10.09%; greater than 0.4 less than 0.5 accounted for 4.26%; greater than 0.5 accounted for 2.71%. Most of the high-hazard events occurred after 2000. the most dangerous DHCEEs ($H = 0.6239$) occurred in July 2001.

Comprehensive, accurate, and rapid analysis of compound hazard intensity and risk is essential for effective agro-meteorological hazard risk management. Given the nutritional value, economic value, and widespread cultivation of maize, our study can provide guiding information with broad implications for future studies on the distribution of compound extreme events and risk assessment. Also, it can be extended to studies on the assessment of the risk of compound extreme events for other crops including but not limited to food crops.

Formatting of funding sources

This study was supported by the National Natural Science Foundation of China (U21A2040), the National K&D Program of China (2022YFD2300201), the National Natural Science Foundation of China (42077443), Science and Technology Development Planning of Jilin Province (20210203153SF) , the Key Scientific and Technology Research and Development Program of Jilin Province (20200403065SF), the Construction Project of the Science and Technology Innovation Center (20210502008ZP).

Author statement

Guo Ying: Conceptualization; Writing Original Draft; Writing Review and Editing; Methodology; Visualization.

Zhang Jiquan*: Funding acquisition. Conceptualization; Writing Review and Editing.

Li Kaiwei: Methodology; Formal analysis; Writing Review Editing.

Aru Han: Software; Visualization.

Feng Zhi: Software.

Liu Xingpeng: Resources.

Tong Zhijun: Funding acquisition.

Declaration of competing interest

The authors declare that they have no known competing financial interests or personal relationships that could have appeared to influence the work reported in this paper.

Data availability

The authors do not have permission to share data.

Appendix A. Supplementary data

Supplementary data to this article can be found online at https://doi.org/10.1016/j.wace.2023.100566.

References

Aas, K., Czado, C., Frigessi, A., Bakken, H., 2009. Pair-copula constructions of multiple dependence. Insur. Math. Econ. 44 (2), 182–198. https://doi.org/10.1016/j.insmatheco.2007.02.001.

Ari, G., Bao, Y., Asi, H., Zhang, J., Na, L., Angge, L., Bao, Y., Han, A., Dong, Z., ZhijunTong, Liu, X., 2021. Impact of global warming on meteorological drought: a case study of the Songliao Plain, China. Theor. Appl. Climatol. 146 (3–4), 1315–1334. https://doi.org/10.1007/s00704-021-03775-x.

Ayub, M., Ashraf, M.Y., Kausar, A., Saleem, S., Anwar, S., Altay, V., Ozturk, M., 2021. Growth and physio-biochemical responses of maize (Zea mays L.) to drought and heat stresses. Plant Biosyst. 155 (3), 535–542. https://doi.org/10.1080/11263504.2020.1762785.

Bastos, A., Ciais, P., Friedlingstein, P., Sitch, S., Pongratz, J., Fan, L., Wigneron, J.P., Weber, U., Reichstein, M., Fu, Z., Anthoni, P., Arneth, A., Haverd, V., Jain, A.K., Joetzjer, E., Knauer, J., Lienert, S., Loughran, T., McGuire, P.C., et al., 2020. Direct and seasonal legacy effects of the 2018 heat wave and drought on European ecosystem productivity. Sci. Adv. 6 (24), 1–14. https://doi.org/10.1126/sciadv.aba2724.

Bin, Z., Lin, F., Xinyu, Z., 2020. Study on Farmers'Ecological compensation behavior in the corn belt of Songliao Plain——taking Jilin Province as an example. J. Northeast Agric. Sci. 45 (1), 54–58. https://doi.org/10.16423/j.cnki.1003-8701.2020.01.012 (In Chinese).

Chunyi, W., Jiquan, Z., Zhiguo, H., Jingjing, C., Xingpeng, L., Qi, Z., 2015. Prospects and progresses in the research of risk assessment of agro-meteorological disasters. Acta Meteorol. Sin. 73 (1), 1–19 (In Chinese).

Cui, P., Peng, J., Shi, P., Tang, H., Ouyang, C., Zou, Q., Liu, L., Li, C., Lei, Y., 2021. Scientific challenges of research on natural hazards and disaster risk. Geograph. Sustain. 2 (3), 216–223. https://doi.org/10.1016/j.geosus.2021.09.001.

Curt, C., 2021. Multirisk: what trends in recent works? – a bibliometric analysis. Sci. Total Environ. 763, 142951 https://doi.org/10.1016/j.scitotenv.2020.142951.

Dai, A., 2013. Increasing drought under global warming in observations and models. Nat. Clim. Change 3 (1), 52–58. https://doi.org/10.1038/nclimate1633.

Damalas, A., Mettas, C., Evagorou, E., Giannecchini, S., Iasio, C., Papadopoulos, M., Konstantinou, A., Hadjimitsis, D., 2018. Development and Implementation of a DECATASTROPHIZE platform and tool for the management of disasters or multiple hazards. Int. J. Disaster Risk Reduc. 31 (May), 589–601. https://doi.org/10.1016/j.ijdrr.2018.05.011.

Danjun, L., Jiquan, Z., Enliang, G., Rui, W., 2017. Identification of drought and drought hazard assessment in midwest of J ilin Province based on SVDI. Bull. Soil Water Conserv. 37 (4), 321–326 (In Chinese).

Dinpashoh, Y., Mirabbasi, R., Jhajharia, D., Abianeh, H.Z., Mostafaeipour, A., 2014. Effect of short-term and long-term persistence on identification of temporal trends. J. Hydrol. Eng. 19 (3), 617–625. https://doi.org/10.1061/(asce)he.1943-5584.0000819.

El Sabagh, A., Hossain, A., Barutçular, C., Islam, M.S., Awan, S.I., Galal, A., Iqbal, M.A., Sytar, O., Yildirim, M., Meena, R.S., Fahad, S., Najeeb, U., Konuskan, O., Habib, R.A., Llanes, A., Hussain, S., Farooq, M., Hasanuzzaman, M., Abdelaal, K.H., et al., 2019. Wheat (Triticum aestivum l.) production under drought and heat stress – adverse effects, mechanisms and mitigation: a review. Appl. Ecol. Environ. Res. 17 (4), 8307–8332. https://doi.org/10.15666/aeer/1704_83078332.

Eyshi Rezaei, E., Webber, H., Gaiser, T., Naab, J., Ewert, F., 2015. Heat stress in cereals: mechanisms and modelling. Eur. J. Agron. 64, 98–113. https://doi.org/10.1016/j.eja.2014.10.003.

Guna, A., Zhang, J., Tong, S., Bao, Y., Han, A., Li, K., 2019. Effect of climate change on maize yield in the growing season: a case study of the Songliao Plain maize belt. Water (Switzerland) 11 (10). https://doi.org/10.3390/w11102108.

Guo, Y., Lu, X., Zhang, J., Li, K., Wang, R., Rong, G., Liu, X., Tong, Z., 2022. Joint analysis of drought and heat events during maize (Zea mays L.) growth periods using copula and cloud models: a case study of Songliao Plain. Agric. Water Manag. 259 (September 2021), 107238 https://doi.org/10.1016/j.agwat.2021.107238.

Hammer, G.L., McLean, G., van Oosterom, E., Chapman, S., Zheng, B., Wu, A., Doherty, A., Jordan, D., 2020. Designing crops for adaptation to the drought and high-temperature risks anticipated in future climates. Crop Sci. 60 (2), 605–621. https://doi.org/10.1002/csc2.20110.

Hao, Z., Singh, V.P., 2020. Compound events under global warming: a dependence perspective. J. Hydrol. Eng. 25 (9), 03120001 https://doi.org/10.1061/(ASCE)HE.1943-5584.0001991.

Haqiqi, I., Grogan, D.S., Hertel, T.W., Schlenker, W., 2021. Quantifying the impacts of compound extremes on agriculture. Hydrol. Earth Syst. Sci. 25 (2), 551–564. https://doi.org/10.5194/hess-25-551-2021.

Huo, Zhiguo, Zhang, Haiyan, Li, Chunhui, Kong, Rui, Jiang, Mengyuan, 2023. Review on high temperature heat damage of maize in China. Journal of Applied Meteorological Science 34 (1), 1–14. https://doi.org/10.11898/1001-7313.20230101 (In Chinese).

Hussain, H.A., Men, S., Hussain, S., Chen, Y., Ali, S., Zhang, S., Zhang, K., Li, Y., Xu, Q., Liao, C., Wang, L., 2019. Interactive effects of drought and heat stresses on morpho-physiological attributes, yield, nutrient uptake and oxidative status in maize hybrids. Sci. Rep. 9 (1), 1–12. https://doi.org/10.1038/s41598-019-40362-7.

Jia, M., Mei-juan, Q., Yu, G., Jing-quan, R.E.N., Yang, L., 2018. Applicability of five drought indices for agricultural drought evaluation in Jilin Province , China. Chin. J. Appl. Ecol. 29 (8), 2624–2632, 10 . 13287/j. (In Chinese).

Jiang, W., Yuan, L., Wang, W., Cao, R., Zhang, Y., Shen, W., 2015. Spatio-temporal analysis of vegetation variation in the Yellow river basin. Ecol. Indicat. 51, 117–126. https://doi.org/10.1016/j.ecolind.2014.07.031.

Kappes, M.S., Keiler, M., von Elverfeldt, K., Glade, T., 2012. Challenges of analyzing multi-hazard risk: a review. Nat. Hazards 64 (2), 1925–1958. https://doi.org/10.1007/s11069-012-0294-2.

Lee, S. hyeok, Kang, J.E., Park, C.S., Yoon, D.K., Yoon, S., 2020. Multi-risk assessment of heat waves under intensifying climate change using Bayesian Networks. Int. J. Disaster Risk Reduc. 50 (May), 101704 https://doi.org/10.1016/j.ijdrr.2020.101704.

Leng, G., Hall, J., 2019. Crop yield sensitivity of global major agricultural countries to droughts and the projected changes in the future. Sci. Total Environ. 654, 811–821. https://doi.org/10.1016/j.scitotenv.2018.10.434.

Li, E., Zhao, J., Pullens, J.W.M., Yang, X., 2022. The compound effects of drought and high temperature stresses will be the main constraints on maize yield in Northeast China. Sci. Total Environ. 812 https://doi.org/10.1016/j.scitotenv.2021.152461.

Li, X., Zhou, W., Chen, Y.D., 2015. Assessment of regional drought trend and risk over China: a drought climate division perspective. J. Clim. 28 (18), 7025–7037. https://doi.org/10.1175/JCLI-D-14-00403.1.

Li, Y.J., Lyu, H.Q., 2022. Effect of agricultural meteorological disasters on the production corn in the Northeast China. Acta Agron. Sin. 48 (6), 1537–1545. https://doi.org/10.3724/SP.J.1006.2022.03061 (In Chinese).

Liu, Y., Zhu, Y., Ren, L., Yong, B., Singh, V.P., Yuan, F., Jiang, S., Yang, X., 2019. On the mechanisms of two composite methods for construction of multivariate drought indices. Sci. Total Environ. 647, 981–991. https://doi.org/10.1016/j.scitotenv.2018.07.273.

Lizaso, J.I., Ruiz-Ramos, M., Rodríguez, L., Gabaldon-Leal, C., Oliveira, J.A., Lorite, I.J., Sánchez, D., García, E., Rodríguez, A., 2018. Impact of high temperatures in maize: phenology and yield components. Field Crop. Res. 216 (June 2017), 129–140. https://doi.org/10.1016/j.fcr.2017.11.013.

Lobell, D.B., Hammer, G.L., Chenu, K., Zheng, B., Mclean, G., Chapman, S.C., 2015. The shifting influence of drought and heat stress for crops in northeast Australia. Global Change Biol. 21 (11), 4115–4127. https://doi.org/10.1111/gcb.13022.

Lyakh, V.A., Kravchenko, A.N., Soroka, A.I., Dryuchina, E.N., 1991. Effects of high temperatures on mature pollen grains in wild and cultivated maize accessions. Euphytica 55 (3), 203–207. https://doi.org/10.1007/BF00021240.

Martens, B., Miralles, D.G., Lievens, H., Van Der Schalie, R., De Jeu, R.A.M., Fernández-Prieto, D., Beck, H.E., Dorigo, W.A., Verhoest, N.E.C., 2017. GLEAM v3: satellite-based land evaporation and root-zone soil moisture. Geosci. Model Dev. (GMD) 10 (5), 1903–1925. https://doi.org/10.5194/gmd-10-1903-2017.

Mayer, L.I., Rattalino Edreira, J.I., Maddonni, G.A., 2014. Oil yield components of maize crops exposed to heat stress during early and late Grain-Filling stages. Crop Sci. 54 (5), 2236–2250. https://doi.org/10.2135/cropsci2013.11.0795.

Mehrabi, Z., Ramankutty, N., 2017. The cost of heat waves and droughts for global crop production. bioRxiv 1–8.

Merz, B., Kuhlicke, C., Kunz, M., Pittore, M., Babeyko, A., Bresch, D.N., Domeisen, D.I.V., Feser, F., Koszalka, I., Kreibich, H., Pantillon, F., Parolai, S., Pinto, J.G., Punge, H.J., Rivalta, E., Schröter, K., Strehlow, K., Weisse, R., Wurpts, A., 2020. Impact forecasting to support emergency management of natural hazards. Rev. Geophys. 58 (4), 1–52. https://doi.org/10.1029/2020RG000704.

Min, J., Ji, L., Pengshi, C., Yang, W., Dongming, L., 2019. Analysis of circulation characteristics and cause of anomalous high temperature and drought in summer of 2018 over Liaoning. Trans Atmos Sci 42 (4), 10. 13878/j . cnki . dqkxxb . 20190326001 (In Chinese).

Minoli, S., Jägermeyr, J., Asseng, S., Urfels, A., Müller, C., 2022. Global crop yields can be lifted by timely adaptation of growing periods to climate change. Nat. Commun. 13 (1), 1–10. https://doi.org/10.1038/s41467-022-34411-5.

Mirabbasi, R., Fakheri-Fard, A., Dinpashoh, Y., 2012. Bivariate drought frequency analysis using the copula method. Theor. Appl. Climatol. 108 (1–2), 191–206. https://doi.org/10.1007/s00704-011-0524-7.

Miralles, D.G., Holmes, T.R.H., De Jeu, R.A.M., Gash, J.H., Meesters, A.G.C.A., Dolman, A.J., 2011. Global land-surface evaporation estimated from satellite-based observations. Hydrol. Earth Syst. Sci. 15 (2), 453–469. https://doi.org/10.5194/hess-15-453-2011.

Narasimhan, B., Srinivasan, R., 2005. Development and evaluation of soil moisture deficit index (SMDI) and evapotranspiration deficit index (ETDI) for agricultural drought monitoring. Agric. For. Meteorol. 133 (1–4), 69–88. https://doi.org/10.1016/j.agrformet.2005.07.012.

Qaseem, M.F., Qureshi, R., Shaheen, H., 2019. Effects of pre-anthesis drought, heat and their combination on the growth, yield and physiology of diverse wheat (Triticum aestivum L.) genotypes varying in sensitivity to heat and drought stress. Sci. Rep. 9 (1), 1–12. https://doi.org/10.1038/s41598-019-43477-z.

Sadegh, M., Ragno, E., AghaKouchak, A., 2017. Multivariate copula analysis toolbox (MvCAT): describing dependence and underlying uncertainty using a bayesian framework. Water Resour. Res. 53 (6), 5166–5183. https://doi.org/10.1002/2016WR020242.

Salvadori, G., De Michele, C., 2004. Frequency analysis via copulas: theoretical aspects and applications to hydrological events. Water Resour. Res. 40 (12), 1–17. https://doi.org/10.1029/2004WR003133.

Salvadori, G., De Michele, C., 2010. Multivariate multiparameter extreme value models and return periods: a copula approach. Water Resour. Res. 46 (10), 219–233. https://doi.org/10.1029/2009WR009040.

Salvadori, G., De Michele, C., Durante, F., 2011. On the return period and design in a multivariate framework. Hydrol. Earth Syst. Sci. 15 (11), 3293–3305. https://doi.org/10.5194/hess-15-3293-2011.

Salvadori, G., Durante, F., De Michele, C., 2013. Multivariate return period calculation via survival functions. Water Resour. Res. 49 (4), 2308–2311. https://doi.org/10.1002/wrcr.20204.

Sánchez, B., Rasmussen, A., Porter, J.R., 2014. Temperatures and the growth and development of maize and rice: a review. Global Change Biol. 20 (2), 408–417. https://doi.org/10.1111/gcb.12389.

Serrano-Notivoli, R., Beguería, S., Saz, M.Á., de Luis, M., 2018. Recent trends reveal decreasing intensity of daily precipitation in Spain. Int. J. Climatol. 38 (11), 4211–4224. https://doi.org/10.1002/joc.5562.

Sheffield, J., Andreadis, K.M., Wood, E.F., Lettenmaier, D.P., 2009. Global and continental drought in the second half of the twentieth century: severity-area-duration analysis and temporal variability of large-scale events. J. Clim. 22 (8), 1962–1981. https://doi.org/10.1175/2008JCLI2722.1.

Shi, Z., Jia, G., Zhou, Y., Xu, X., Jiang, Y., 2021. Amplified intensity and duration of heatwaves by concurrent droughts in China. Atmos. Res. 261 (April), 105743 https://doi.org/10.1016/j.atmosres.2021.105743.

Siebers, M.H., Slattery, R.A., Yendrek, C.R., Locke, A.M., Drag, D., Ainsworth, E.A., Bernacchi, C.J., Ort, D.R., 2017. Simulated heat waves during maize reproductive stages alter reproductive growth but have no lasting effect when applied during vegetative stages. Agric. Ecosyst. Environ. 240, 162–170. https://doi.org/10.1016/j.agee.2016.11.008.

Teixeira, E.I., Fischer, G., Van Velthuizen, H., Walter, C., Ewert, F., 2013. Global hot-spots of heat stress on agricultural crops due to climate change. Agric. For. Meteorol. 170, 206–215. https://doi.org/10.1016/j.agrformet.2011.09.002.

Ting-ting, W., Hong-yan, Z., Xiao-yi, G., Zheng-xiang, Z., Jian-jun, Z., 2014. Spatiotemporal change of drought over the Songliao Plain based on TVDI. Arid Zone Res. 31 (3), 3–9. https://doi.org/10.13866/j.azr.2014.03.029 (In Chinese).

Wang, J., He, Z., Weng, W., 2020. A review of the research into the relations between hazards in multi-hazard risk analysis. Nat. Hazards 104 (3), 2003–2026. https://doi.org/10.1007/s11069-020-04259-3.

Wang, L., Liao, S., Huang, S., Ming, B., Meng, Q., Wang, P., 2018. Increasing concurrent drought and heat during the summer maize season in Huang–Huai–Hai Plain, China. Int. J. Climatol. 38 (7), 3177–3190. https://doi.org/10.1002/joc.5492.

Wang, W., Zhang, Y., Guo, B., Ji, M., Xu, Y., 2021. Compound droughts and heat waves over the huai river basin of China: from a perspective of the magnitude index. J. Hydrometeorol. 22 (11), 3107–3119. https://doi.org/10.1175/JHM-D-20-0305.1.

Wang, Z., Sun, J., Du, Y., Niu, W., 2022. Conservation tillage improves the yield of summer maize by regulating soil water, photosynthesis and inferior kernel grain filling on the semiarid Loess Plateau, China. J. Sci. Food Agric. 102 (6), 2330–2341. https://doi.org/10.1002/jsfa.11571.

Waqas, M.A., Wang, X., Zafar, S.A., Noor, M.A., Hussain, H.A., Azher Nawaz, M., Farooq, M., 2021. Thermal stresses in maize: effects and management strategies. Plants 10 (2), 1–23. https://doi.org/10.3390/plants10020293.

Ward, P.J., Blauhut, V., Bloemendaal, N., Daniell, E.J., De Ruiter, C.M., Duncan, J.M., Emberson, R., Jenkins, F.S., Kirschbaum, D., Kunz, M., Mohr, S., Muis, S., Riddell, A. G., Schäfer, A., Stanley, T., Veldkamp, I.E.T., Hessel, W.C., 2020. Review article:

natural hazard risk assessments at the global scale. Nat. Hazards Earth Syst. Sci. 20 (4), 1069–1096. https://doi.org/10.5194/nhess-20-1069-2020.

Wilhelm, E.P., Mullen, R.E., Keeling, P.L., Singletary, G.W., 1999. Heat stress during grain filling in maize: effects on kernel growth and metabolism. Crop Sci. 39 (6), 1733–1741. https://doi.org/10.2135/cropsci1999.3961733x.

Wu, X., Hao, Z., Hao, F., Singh, V.P., Zhang, X., 2019. Dry-hot magnitude index: a joint indicator for compound event analysis. Environ. Res. Lett. 14 (6) https://doi.org/10.1088/1748-9326/ab1ec7.

Xi, Z.-X., 2001. Weather characteristics and impacts of summer 2001 (June-August) in Jilin Province. JILIN QIXIANG 4, 19–20 (In Chinese).

Xin-ying, X., Chang-xiu, S., Zhi-gang, S., Bu-ju, L., Wan-lin, D., 2021. Research progress on the effect of heat stress on physiological characteristics of maize at key growth stage and the yield. Journal of Maize Sciences 29 (2). https://doi.org/10.13597/j.cnki.maize.science.20210213 (In Chinese).

Ye, L., Shi, K., Xin, Z., Wang, C., Zhang, C., 2019. Compound droughts and heat waves in China. Sustainability 11 (12), 3270. https://doi.org/10.3390/su11123270.

Yue, Y., Shen, S. he, Wang, Q., 2018. Trend and variability in droughts in Northeast China based on the reconnaissance drought index. Water (Switzerland) 10 (3). https://doi.org/10.3390/w10030318.

Zargar, A., Sadiq, R., Naser, B., Khan, F.I., 2011. A review of drought indices. Environ. Rev. 19 (1), 333–349. https://doi.org/10.1139/a11-013.

Zhang, J., Hayakawa, S., 1999. Risk assessment and classification of drought injury to maize in Songliao Plain, China. J. Agric. Meteorol. 55 (1), 1–13. https://doi.org/10.2480/agrmet.55.1.

Zhang, Q., Han, J., Yang, Z., 2021. Hazard assessment of extreme heat during summer maize growing season in Haihe Plain, China. Int. J. Climatol. 41 (10), 4794–4803. https://doi.org/10.1002/joc.7099.

Zhang, Z., Yang, X., Liu, Z., Bai, F., Sun, S., Nie, J., Gao, J., Ming, B., Xie, R., Li, S., 2020. Spatio-temporal characteristics of agro-climatic indices and extreme weather events during the growing season for summer maize (Zea mays L.) in Huanghuaihai region, China. Int. J. Biometeorol. 64 (5), 827–839. https://doi.org/10.1007/s00484-020-01872-6.

Zhu, P., Jin, Z., Zhuang, Q., Ciais, P., Bernacchi, C., Wang, X., Makowski, D., Lobell, D., 2018. The important but weakening maize yield benefit of grain filling prolongation in the US Midwest. Global Change Biol. 24 (10), 4718–4730. https://doi.org/10.1111/gcb.14356.

Zhu, P., Zhuang, Q., Archontoulis, S.V., Bernacchi, C., Müller, C., 2019. Dissecting the nonlinear response of maize yield to high temperature stress with model-data integration. Global Change Biol. 25 (7), 2470–2484. https://doi.org/10.1111/gcb.14632.